Tailoring MOF structure via ligand optimization achieved dandelion flower like CoS/Co-Nx/CoNi/NiS catalyst to enhance ORR/OER for zinc-air batteries

Mohan Gopalakrishnan[1], Mohamad Etesami[1], Jayaraman Theerthagiri[2], Myong Yong Choi[2], Suttipong Wannapaiboon[3], Mai Thanh Nguyen[4], Tetsu Yonezawa[4], Soorathep Kheawhom[1,5,6,*]

[1]Department of Chemical Engineering, Faculty of Engineering, Chulalongkorn University, Bangkok 10330, Thailand

[2]Core-Facility Center for Photochemistry & Nanomaterials, Department of Chemistry (BK21 FOUR), Research Institute of Natural Sciences, Gyeongsang National University, Jinju 52828, Republic of Korea

[3]Synchrotron Light Research Institute, 111 University Avenue, Muang District, Nakhon Ratchasima 30000, Thailand

[4]Division of Materials Science and Engineering, Faculty of Engineering, Hokkaido University, Hokkaido 060-8628, Japan

[5]Bio-Circular-Green-economy Technology & Engineering Center (BCGeTEC), Faculty of Engineering, Chulalongkorn University, Bangkok 10330, Thailand

[6]Center of Excellence on Advanced Materials for Energy Storage, Chulalongkorn University, Bangkok 10330, Thailand

Corresponding author: soorathep.k@chula.ac.th

Supporting Information

1. Synthesis of 4-aminodiacetic terephthalic acid

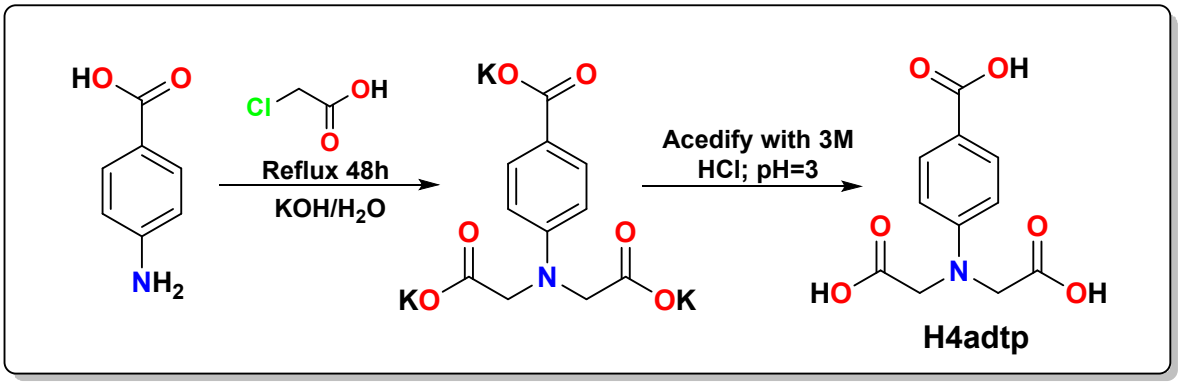

Scheme S1. Synthesis of 4-aminodiacetic terephthalic acid from 4-aminobenzoic acid.

The ligand H4adtp was synthesized by the flowing procedure. A solution of KOH (16.8 g, 0.3 mol) in water (100 mL) was added dropwise to a solution of chloroacetic acid (14.2 g, 0.15 mol) in water (100 mL). *p*-Aminobenzoic acid (6.9g, 0.1 mol) was slowly added to the resulting alkaline solution, and the mixture was refluxed at 80 °C for 30 h. The reaction mixture was then cooled to room temperature and acidified with HCl (3M) until the desired acid precipitated as a pale-yellow solid (pH 2.5) (Scheme S1). This precipitated was collected by filtration, washed with water, and recrystallized from water (yield: 33% based on p-aminobenzoic acid). ^{1}H NMR (300 MHz, DMSO-D_6, 23 °C): δ = 7.84 (d, 2 H, m), 6.58 (d, 2 H, m), 4.23 (s, 4 H, CH_2–COO, s). ^{13}C(300 MHz, DMSO-D_6, 23 °C): δ = 59.95 (2C, NCH_2, m), 111.11 (2C, C-ph, m), 118.1 (1C, ph-COOH, s), 131.04 (2C,C-ph, s), 152.11 (1C-CN, s), 167 (1C-COOH, m), 174.52 (2C-NCH_2COOH, s).

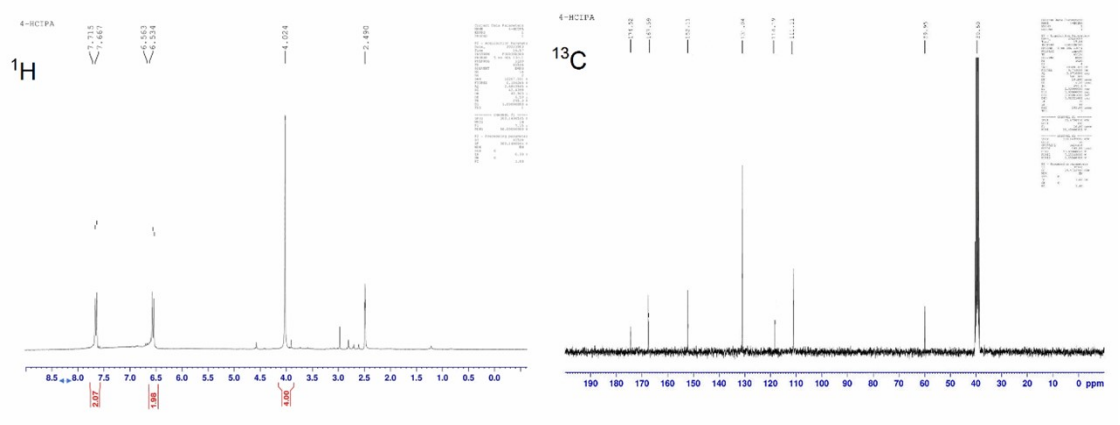

Fig.S1. Both ^{1}H and ^{13}C NMR spectra of 4-aminodiacetic terephthalic acid in DMSO-D_6.

2. Electrocatalyst characterization

Field emission scanning electron microscopy (FE-SEM, JEOL JSM-7800F), transmission electron microscopy (TEM, JEOL JM-2010, JEOL JEM-F200), and atomic force microscopy were used to examine the microstructures of the catalysts (AFM, MultiMode8 SPM). The Raman spectra were taken on a Perkin Elmer furrier transform Raman spectrometer at an excitation wavelength of 532 nm. The powder X-ray diffraction (XRD) in the range of 2 (10° 80°) were taken on a Bruker D8 advance diffractometer used to analyze morphology and structure of the samples. X-ray photoelectron spectroscopy (XPS) analyses were performed using a PHI Quantum 2000 scanning ESCA Microprobe spectrometer. The specific surface area was evaluated by the Brunauer-Emmett-Teller (BET) method, which was carried out on Microporous instrument Tristar 3000 at −196 °C. All samples were outgassed for 10 h at 150 °C before measurements to remove any moisture or adsorbed contaminants that might be present on their surfaces.

3. Electrochemical measurements

All the electrochemical tests were carried out on by two potentiostats of VersaSTAT 3F with a traditional with a three-electrode system. The reference electrode was an Hg/HgO solution immersed in 1 M KOH and Pt wire was utilized as the counter electrode. The working electrodes were rotating disk electrodes (RDE, diameter = 3 mm) and rotating ring-disk electrodes (RRDE, glassy carbon diameter = 4 mm and platinum ring diameter = 7 mm) modified by as-prepared electrocatalysts. The functioning electrodes were modified in the following way: To make the slurry, 5 mg of sample with ultrasonically dispersed in 500 µl of ethanol, 500 µl of deionized water, and 20 µl of 10% Nafion. After that, 10 µl of slurries was dropped onto cleansed RDE and RRDE, respectively. The RDE and RRDE were then allowed to dry at ambient temperature. Electrodes changed by all catalysts, on the other hand, were made in the same way. In the test system, the electrolyte was KOH (0.1 mol L^{-1}). Linear sweep voltammetry (LSV) curves were also generated at a scan rate of 10 mV s^{-1}. With the Nernst equation, all potentials were converted to reversible hydrogen electrodes (RHE).

$$E_{RHE} = E_{Hg/HgO} + 0.098V + 0.059\ pH \quad (1)$$

RRDE electrodes were used to assess the electron transfer number (n) and hydrogen peroxide yield (percent H2O2) of CoN/UNG and Pt/C during ORR:

$$n = 4I_d / (I_d + I_r / N)\% \quad (2)$$

$$HO_2^-(\%) = 200(I_r / N) / (I_d + I_r / N) \quad (3)$$

The rotation speed of the electrode was set to 1600 rpm, and all experiments were conducted at 25 °C. At the electrode on the disk (glassy carbon disk, GC disk).

3.1 Oxygen reduction reaction

Glassy carbon (GCE) was coated with catalyst ink using a 0.5 mg cm^2 loading quantity. The reference catalyst used was commercial Pt/C (20 wt%). The LSV curves were measured at a series of rotating electrode speeds (400, 800, 1200, and 1600 rpm) at a scan rate of 10 mV s^{-1} whereas the CV curves were measured in an O_2-saturated 0.1 M KOH aqueous solution at a scan rate of 10 mV s^{-1} at a potential range of 0 to 0.6 V ($E_{Hg/HgO}$). The reversible hydrogen electrode (RHE) was created from each potential using the formula $E_{RHE} = E_{Hg/HgO} + 0.098V + 0.059$ pH

In alkaline medium, the ORR could occur in the following 4-electron reaction pathway:

$$* + O_2\,(g) + H_2O\,(l) + e^- \rightarrow *OOH + OH^- \quad (4)$$

$$*OOH + e- \rightarrow *O + OH^- \quad (5)$$

$$*O + H_2O\,(l) + e^- \rightarrow *OH + OH^- \quad (6)$$

$$*OH + e- \rightarrow * + OH^- \quad (7)$$

3.2. Oxygen evolution reaction

GCE was covered with catalyst ink using a 0.9 mg cm^{-2} loading quantity. The reference catalysts used in this experiment were commercial RuO_2 and RuO_2+Pt/C. First, CV measurements were performed as an activation process in a 0.1 M KOH aqueous solution in the potential range of 0 to 0.6 V (versus Hg/HgO). With a scan rate of 10 mV s^{-1}, the LSV curves were measured from 0 to +1.2 V (versus Hg/HgO). The reversible hydrogen electrode (RHE) was created from each potential using the formula $E_{RHE} = E_{Hg/HgO} + 0.098$ V + 0.0591pH.

In alkaline medium, the OER could occur via a 4-electron reaction pathway:

$$H_2O(l)+* \rightarrow *HO+H^+ + e^- \quad (8)$$

$$*HO \rightarrow *O+H^+ + e^- \quad (9)$$

$$*O+H2O(l) \rightarrow *OOH+H^{++} e^{-} \quad (10)$$

$$*OOH \rightarrow O2(g) + *+H^{++} e- \quad (11)$$

4. Air cathode fabrication

The air electrode was prepared by coating one side of the air electrode with GDL as a hydrophobic layer to prevent electrolyte leakage through the air electrode. GDL was made by combining carbon BP-2000 (0.4 g), PTFE (0.93 g), and 99% ethanol (10 ml) for 2 hr. The coated electrode was hot-pressed for 15 minutes at 350°C. The air electrode was again pressed for 1 minute at room temperature with a pressure of 1000 N/cm^2. The cathode catalyst ink was created by dispersing 10 mg of each sample mixed with 3mg BP2000 carbon blacks in 1 mL of 0.5 percent Nafion solution using sonification. On a pressed nickel foam, 100 µL of 0.5 percent Nafion was applied first, followed by 100 µL of the catalyst ink. The treated nickel foam was then pressed together with a carbon-based GDL and ePTFE to form a cathode as illustrated in Fig. S1.

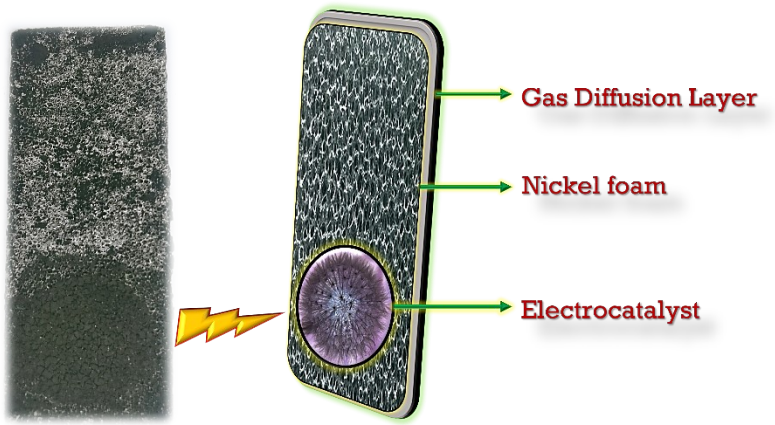

Figure S2. Air cathode fabrication with catalyst Co_9S_8/Co-N_x/CoNi/Ni_3S_2@CNS-**4**

5. Zinc-air battery assembly

Laboratory-scale ZABs were used in full-cell charge and discharge cycling tests (Fig. S2) As anodes, 3 mm thick polished Zn plates were used. Laboratory-scale Zn-air cell was used to assemble and test a liquid Zn-air battery. The exposed control area of the cathode to the electrolyte was 0.7 cm^2. As an aqueous electrolyte, 6.0 M KOH with 0.2 M $Zn(CH_3COO_2)_2$ was used. Cycling tests were performed with a Newar battery tester at 10 mA cm^2 of the cathode (NEWARE, CT-4008-5V 20mA).

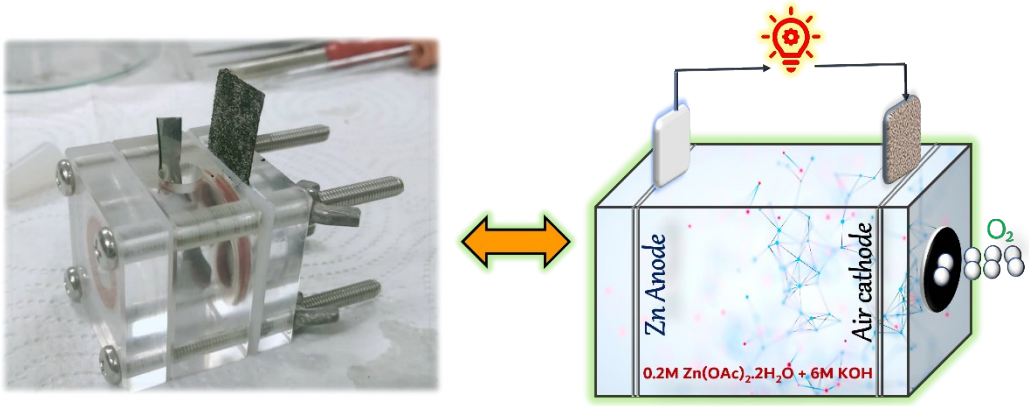

Figure S3. Zinc air battery assembly and their illustration

6. *Supplementary figures*

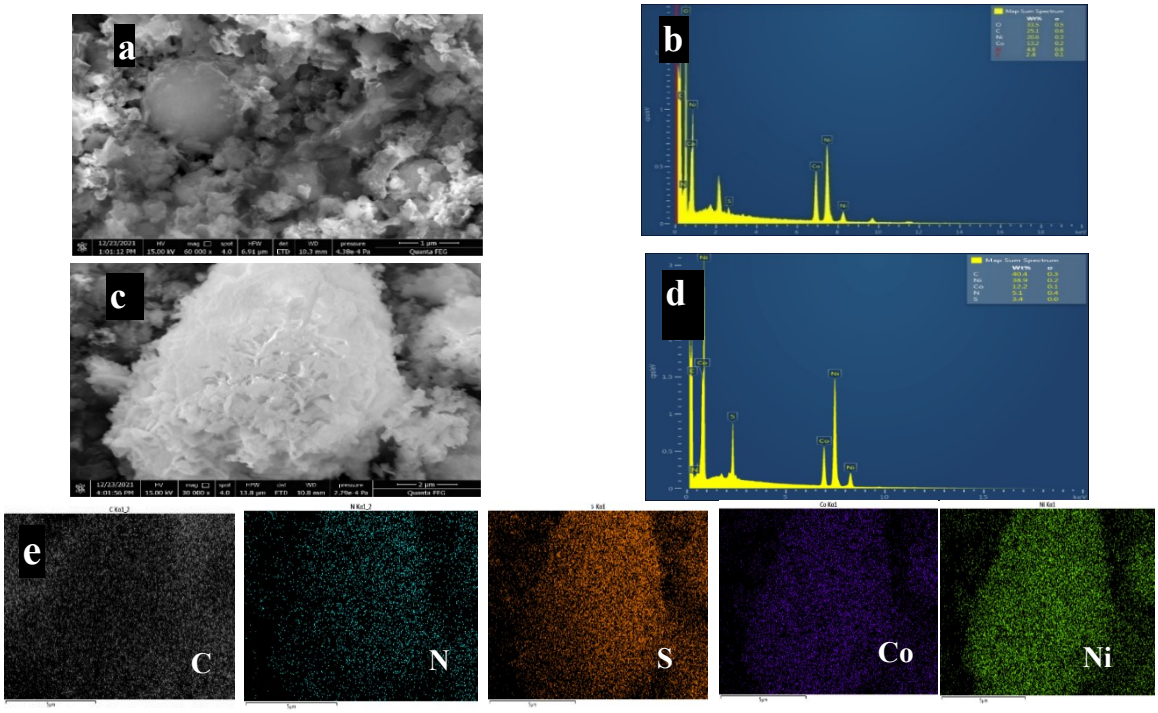

Figure S4. (a,b) SEM and EDAX spectra of the MOF precursor-**2**. (c,d) SEM and EDAX spectrum of Co_9S_8/Co-N_x/CoNi/Ni_3S_2@CNS-**2** after calcination 700 ^oC in Ar. (e) EDS mappings for carbon (C), nitrogen (N), sulphur (S), cobalt (Co) and nickel (Ni).

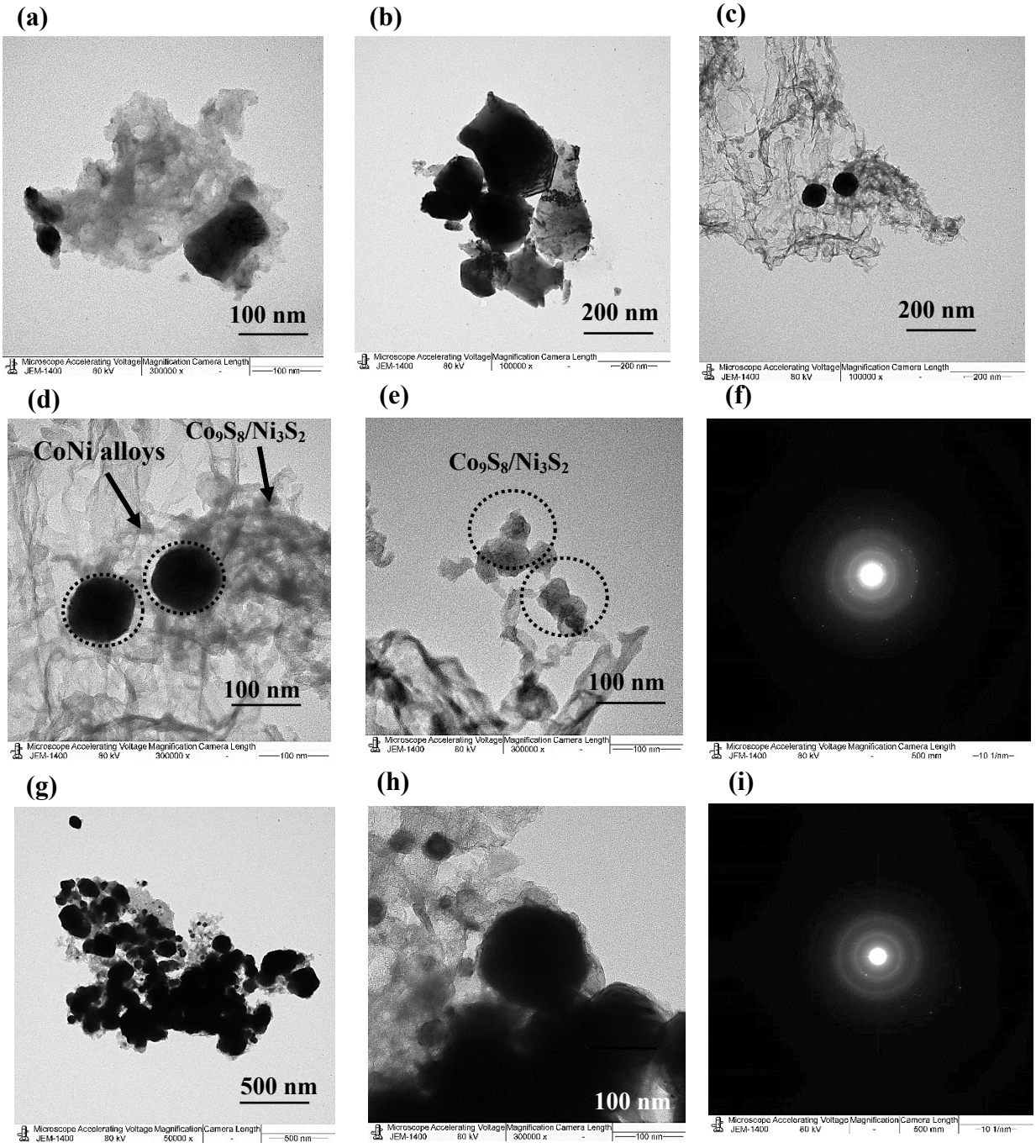

Figure S5. TEM images of electrocatalysts: (a,b) TEM images of Co_9S_8/ CoNi/Ni_3S_2@CNS-**1**. (e-f) TEM images of Co_9S_8/Co-N_x/CoNi/Ni_3S_2@CNS-**2** and Fourier transform SAED pattern. (g-i) TEM images of Co_9S_8/ CoNi/Ni_3S_2@CNS-**3** and Fourier transform SAED pattern.

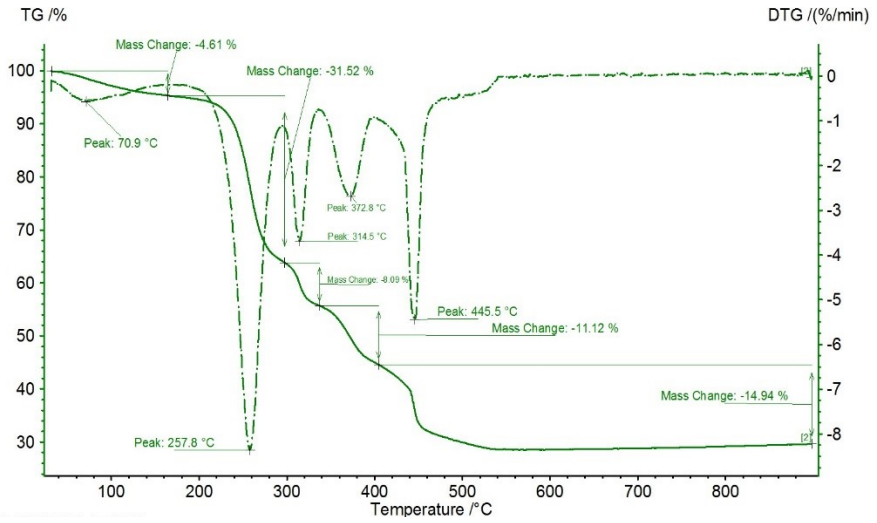

Figure S6. TGA spectrum of MOF precursor-**2** to catalyst Co_9S_8/N-CoNi/Ni_3S_2@CNS-**2** solid state conversation.

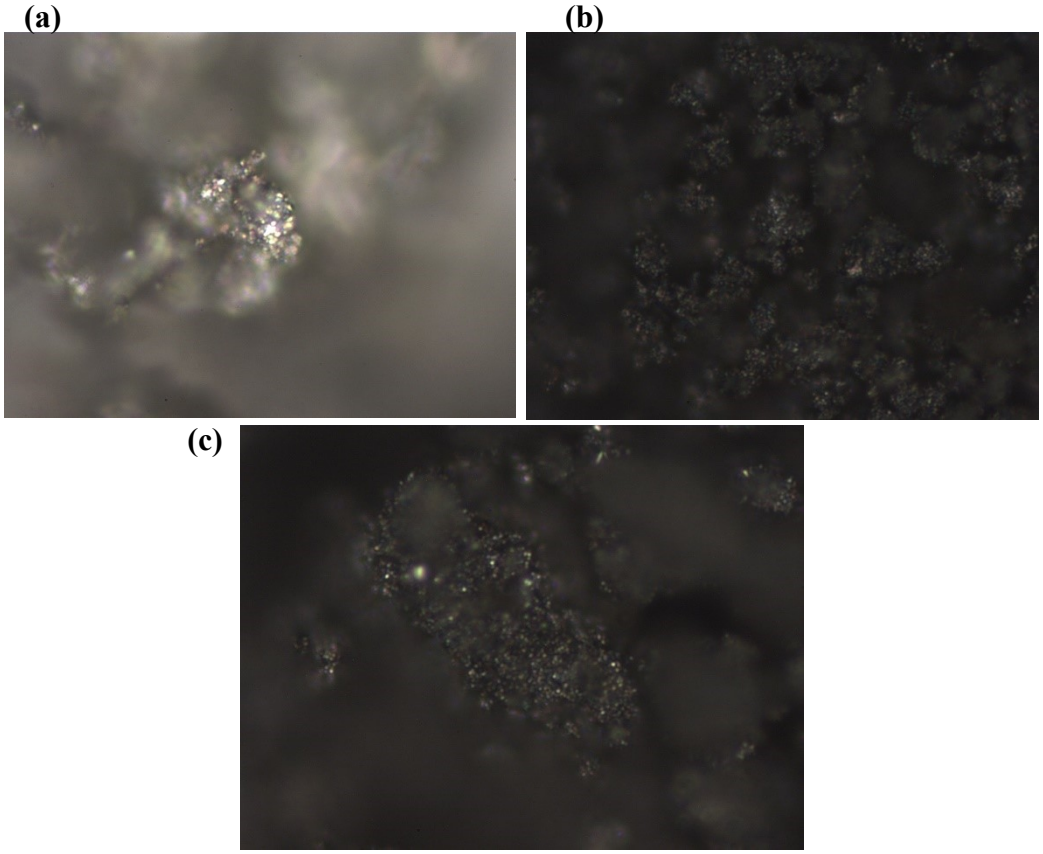

Figure S7. Raman microscopic (laser at 532 nm) images of catalysts Co_9S_8/CoNi/Ni_3S_2@CNS-**1**, Co_9S_8/Co-Nx/CoNi/Ni_3S_2@CNS-**2** and Co_9S_8/CoNi/Ni_3S_2@CNS-**3**.

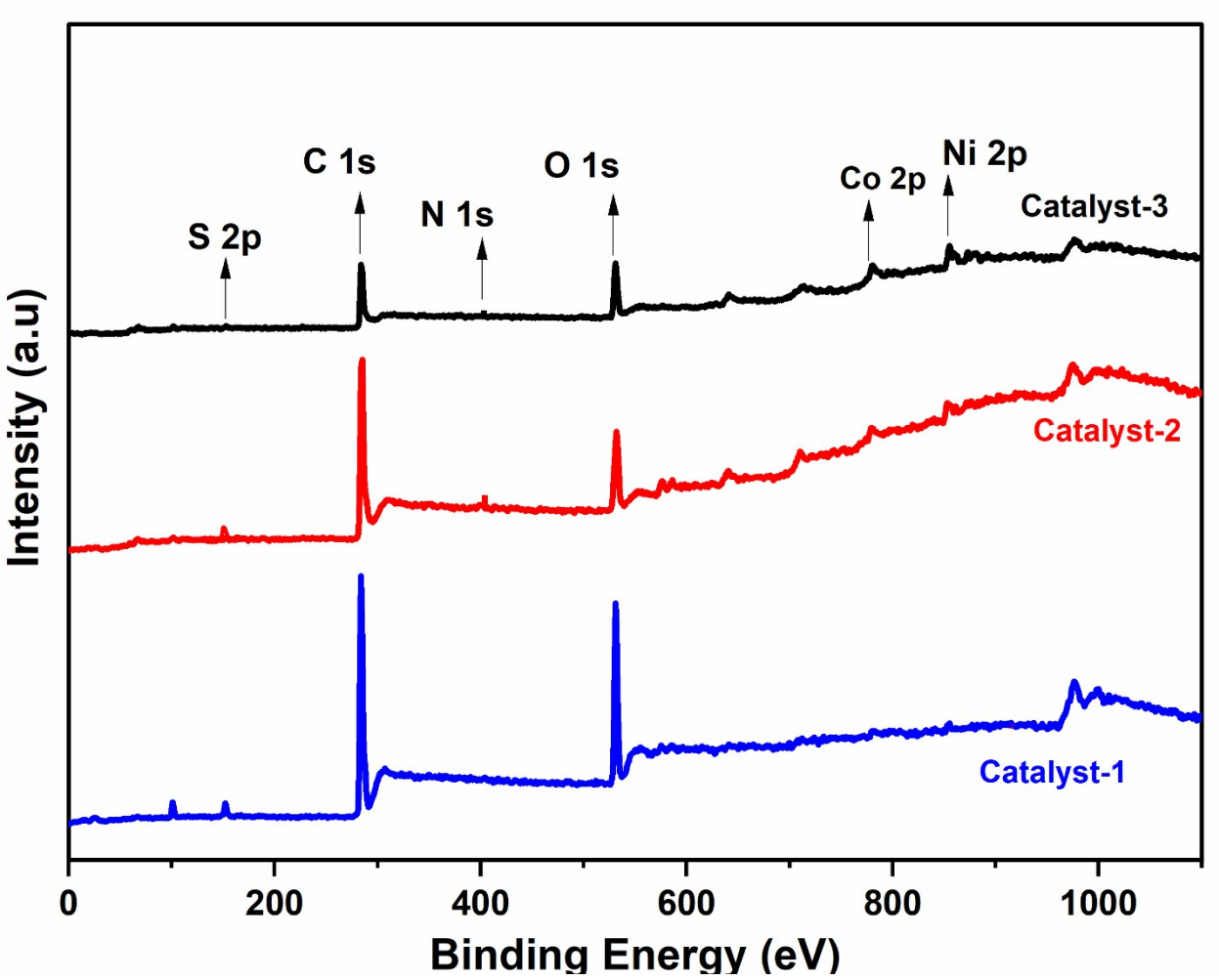

Figure S8. The XPS survey spectrum of catalysts 1-3.

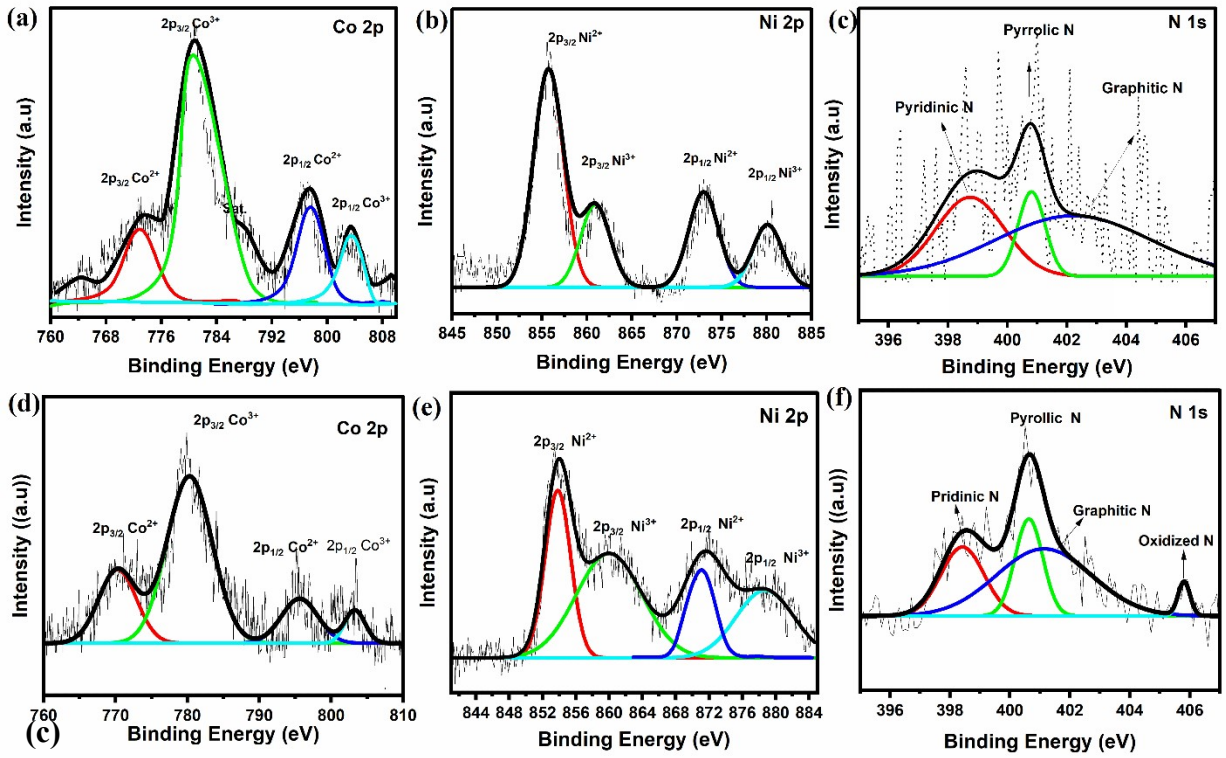

Figure S9. High-resolution XPS spectra of (a-c) Co 2p; Ni 2p; N 1s of Co_9S_8/CoNi/Ni_3S_2@CNS-**1** and (d-f) Co 2p; Ni 2p; N 1s of Co_9S_8/Co-N_x/CoNi/Ni_3S_2@CNS-**2**.

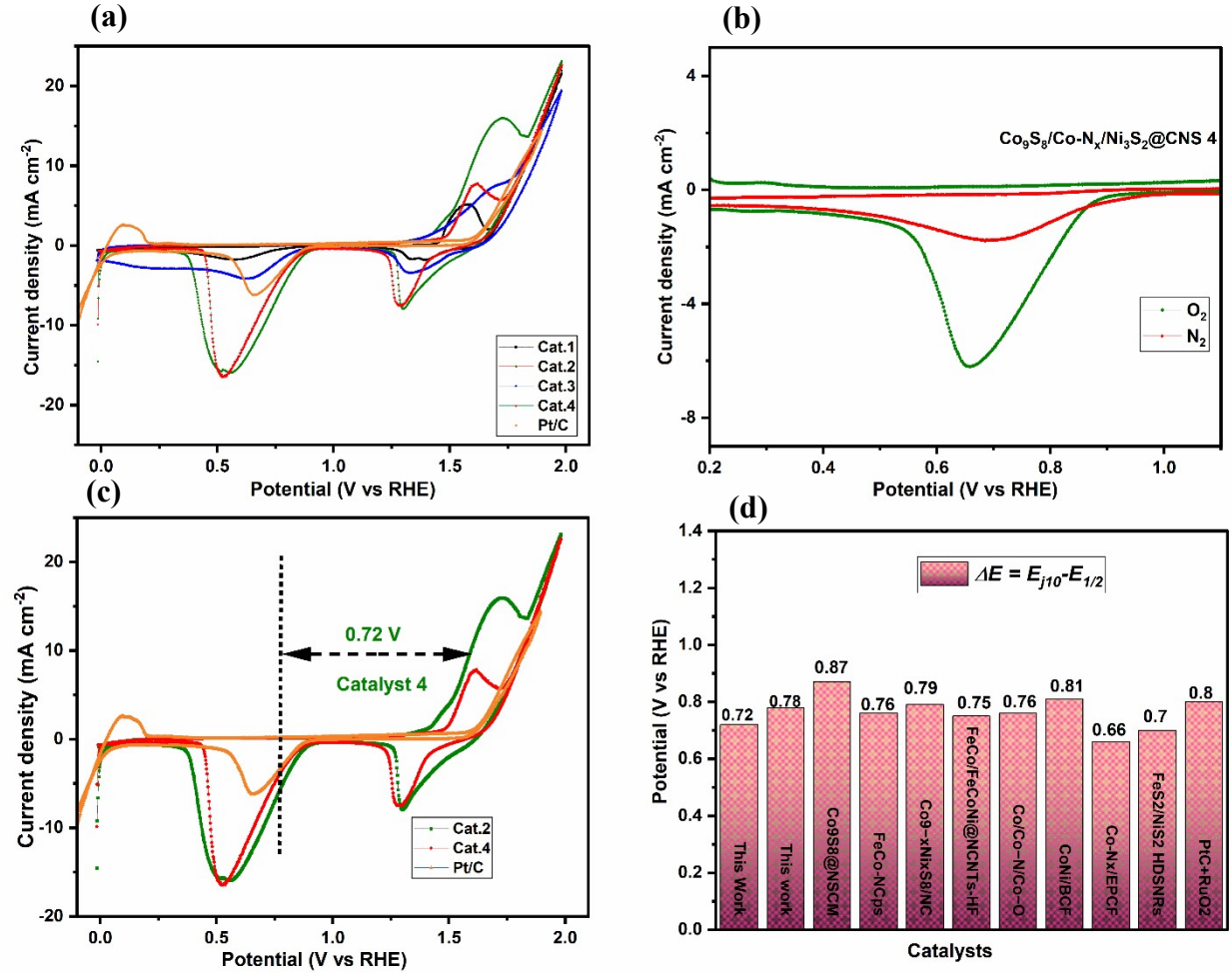

Figure S10. (a) CV curves in O_2 saturated KOH electrolytes for CoS/Co-N_x/CoNi/NiS@CNS **1-4** (b) CV curves in O_2 and N_2-saturated KOH electrolytes for the Co_9S_8/Co-N_x/CoNi/Ni_3S_2@CNS-**4**. (c,d) the ΔE values ($\Delta E = E_{j10} - E_{1/2}$) of the as prepared electrocatalyst, the benchmark Pt/C+RuO_2 with the reported electrocatalysts.

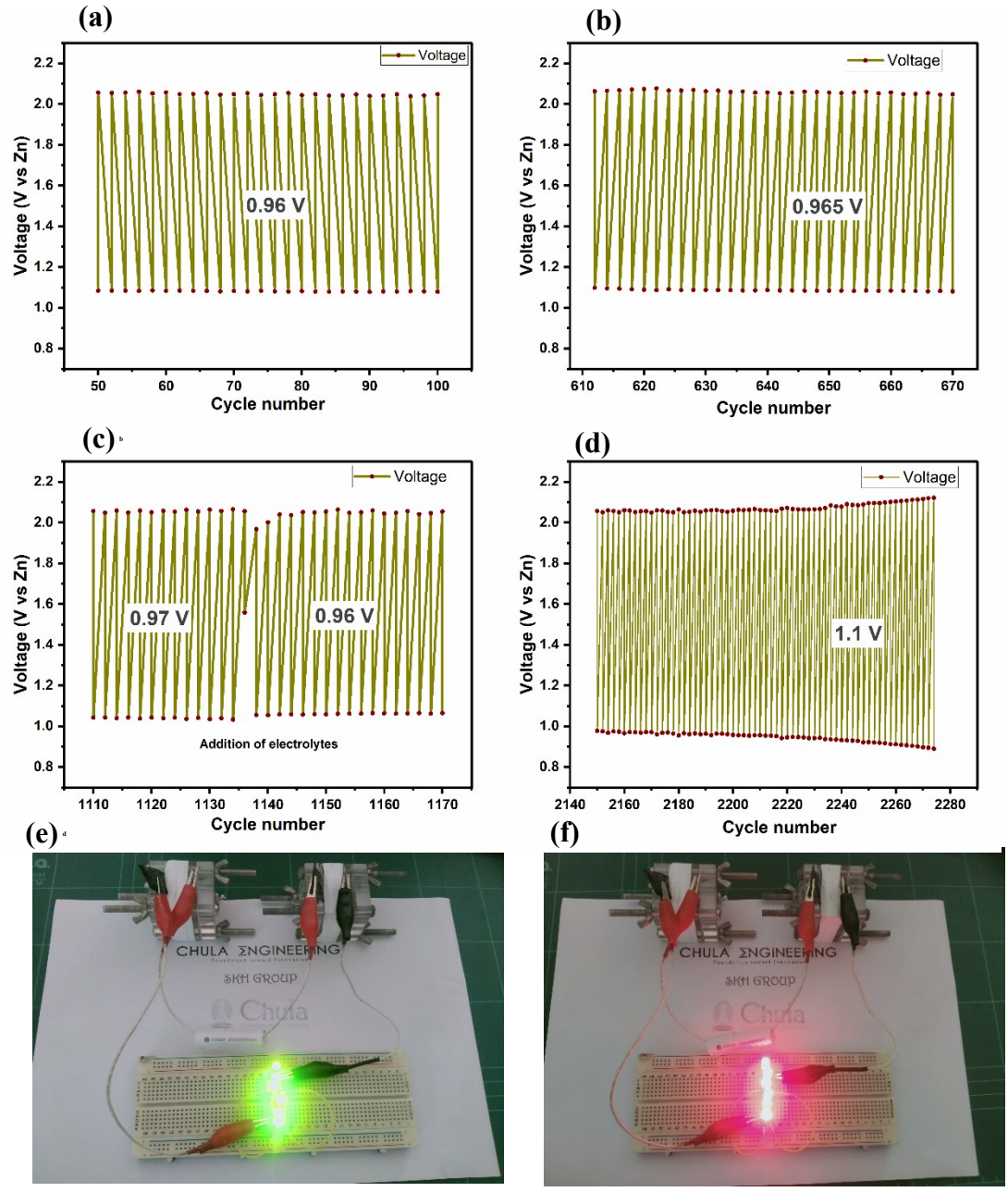

Figure S 11. (a-d) Different charge and discharge polarization curves of the rechargeable ZABs using Co_9S_8/Co-N_x/CoNi/Ni_3S_2@CNS-**4**. (e,f) The photo of two zinc-air batteries connected in series to drive green and red LED lights.

7. Supplementary Tables

Table S1. Comparison of ORR/OER parameters for recent reported electrocatalysts in 0.1KOH electrolyte.

Catalysts	ORR		OER	ΔE (V)	Reference
	$E_{1/2}$ (V)	*n*	E_{j10} (V)		
Co_9S_8/Co-N_x/CoNi/Ni_3S_2-4	0.86	3.98	1.58	0.72	**This work**
Co_9S_8/Co-N_x/CoNi/Ni_3S_2-2	0.83	3.96	1.61	0.78	**This work**
Co_9S_8@NSCM	0.81	4.02	1.72	0.877	[1]
S-$Co_{9-x}Fe_xS_8$@rGO	0.84	3.97	-	-	[2]
FeCo-NCps	0.84	3.81	1.60	0.76	[3]
CoFe/SNC	0.86	3.90	1.59	0.73	[4]
CoS_x	0.80	3.85	1.54	0.74	[5]
$Co_{9-x}Ni_xS_8$/NC	0.86	3.96	1.65	0.79	[6]
FeCo/FeCoNi@NCNTs-HF	0.85	3.98	1.60	0.75	[7]
FeCo/NUCSs	0.88	3.95	1.49	0.62	[8]
CoPi-NPC	0.79	3.80	-	-	[9]
FeS_2/NiS_2 HDSNRs	0.80	3.86	1.50	0.70	[10]
Co/CoS/Fe-HSNC	0.90	4.0	1.50	0.60	[11]
Fe_2P/Co@NPC	0.87	3.9	1.73	0.86	[12]
Ni_3S_2−Co_9S_8/NCAs	-	-	1.60	-	[13]
NiFe@NC	0.86	3.94	1.50	0.64	[14]
Co@bCNTs	0.84	3.93	1.56	0.72	[15]
Co/Co−N/Co−O	0.85	3.98	1.61	0.76	[16]
CoDNG	0.86	3.97	1.58	0.72	[17]
CoNi/BCF	0.80	3.86	1.61	0.81	[18]
NiCo@N–Cs	0.88	3.86	1.51	0.63	[19]
Co-N_x/EPCF	0.87	3.95	1.53	0.66	[20]

Table S2. EIS data of ORR and OER of electrocatalysts **1-4**

Catalysts	ORR		OER	
	Rs (Ω)	Rct (Ω)	Rs (Ω)	Rct (Ω)
Co_9S_8/CoNi/Ni_3S_2@CNS-1	66.5	249.4	70.1	233.9
Co_9S_8/Co-Nx/CoNi/Ni_3S_2@CNS-2	71.4	189.3	62.5	148.2
Co_9S_8/CoNi/Ni_3S_2@CNS-3	75.5	235.3	65.5	166.3
Co_9S_8/Co-Nx/CoNi/Ni_3S_2@CNS-4	69.4	175.4	60.9	144.6

Table S3. A comparison of the performance of Co_9S_8/Co-N_x/CoNi/Ni_3S_2@CNS-**4** ZAB with that of recently reported active catalysts.

Catalysts	Open Circuit Voltage	Power density (mW cm^{-2})	Charge and discharge time(h)	Reference
Co_9S_8/Co-N_x/CoNi/Ni_3S_2@CNS-4	1.59	206.9	435	**This work**
$Fe_{1.2}$Co@NC/NCNTs	1.43	242	155	[3]
CoFe/SNC	1.47	130	100	[4]
$Co_{9-x}Ni_xS_8$/NC	1.45	75	60	[6]
FeCo/FeCoNi@NCNTs-HF	1.48	156.2	200	[7]
FeCo/NUCSs	1.51	152.3	102	[8]
CoPi-NPC	1.41	186	33	[9]
FeS_2/NiS_2 HDSNRs	1.44	130	270	[10]
Co/CoS/Fe-HSNC	1.49	213	30	[11]
CoNi/BCF	1.44	155.1	30	[18]
CoNi-MOF/rGO	1.37	97	120	[21]
CoNi/NHCS-TUC-3	1.59	255.9	71	[22]
CoNiS/NPSC	1.42	156	10	[23]
CoNi/MoC-NP-CTS	1.47	132	160	[24]
Co/Co−N/Co−O	1.47	157	200	[16]
CoNiCN@NC–2–800	1.52	172	300	[25]

References

1. Y. Li, W. Zhou, J. Dong, Y. Luo, P. An, J. Liu, X. Wu, G. Xu, H. Zhang and J. Zhang, *Nanoscale*, 2018, **10**, 2649-2657, DOI: 10.1039/C7NR07235J.
2. T. Liu, F. Yang, G. Cheng and W. Luo, *Small*, 2018, **14**, 1703748, DOI: 10.1002/smll.201703748.
3. J. Liu, T. He, Q. Wang, Z. Zhou, Y. Zhang, H. Wu, Q. Li, J. Zheng, Z. Sun, Y. Lei, J. Ma and Y. Zhang, *Journal of Materials Chemistry A*, 2019, **7**, 12451-12456, DOI: 10.1039/C9TA02264C.
4. G. Li, Y. Tang, T. Fu, Y. Xiang, Z. Xiong, Y. Si, C. Guo and Z. Jiang, *Chem. Eng. J.*, 2022, **429**, 132174, DOI: 10.1016/j.cej.2021.132174.
5. Q. Lu, J. Yu, X. Zou, K. Liao, P. Tan, W. Zhou, M. Ni and Z. Shao, *Adv. Funct. Mater.*, 2019, **29**, 1904481, DOI: 10.1002/adfm.201904481.
6. Z. Cai, I. Yamada and S. Yagi, *ACS Applied Materials & Interfaces*, 2020, **12**, 5847-5856, DOI: 10.1021/acsami.9b19268.
7. Z. Wang, J. Ang, B. Zhang, Y. Zhang, X. Y. D. Ma, T. Yan, J. Liu, B. Che, Y. Huang and X. Lu, *Applied Catalysis B: Environmental*, 2019, **254**, 26-36, DOI: 10.1016/j.apcatb.2019.04.027.
8. X. Xu, J. Xie, B. Liu, R. Wang, M. Liu, J. Zhang, J. Liu, Z. Cai and J. Zou, *Applied Catalysis B: Environmental*, 2022, **316**, 121687, DOI: 10.1016/j.apcatb.2022.121687.
9. P. Thangasamy, S. Oh, H. Randriamahazaka, S. Nam and I.-K. Oh, *Applied Catalysis B: Environmental*, 2022, **316**, 121656, DOI: 10.1016/j.apcatb.2022.121656.
10. L. Wu, J. Li, C. Shi, Y. Li, H. Mi, L. Deng, Q. Zhang, C. He and X. Ren, *Journal of Materials Chemistry A*, 2022, **10**, 16627-16638, DOI: 10.1039/D2TA03554E.
11. L. Yan, H. Wang, J. Shen, J. Ning, Y. Zhong and Y. Hu, *Chem. Eng. J.*, 2021, **403**, 126385, DOI: 10.1016/j.cej.2020.126385.
12. Y. Bai, Y. Wang, Z. Qiao, Y. Yang, L. Deng, C. Li, X. Chen, S. Wang, Y. Huang, X. Zhang and D. Cao, *Journal of Materials Chemistry A*, 2022, **10**, 16037-16045, DOI: 10.1039/D2TA03099C.
13. X. Wang, Y. Yang, R. Wang, L. Li, X. Zhao and W. Zhang, *Langmuir*, 2022, **38**, 7280-7289, DOI: 10.1021/acs.langmuir.2c00805.
14. X. Zhang, J. Wang, C. Dai, X. Jin, Y. Zhao and L. Qu, *J. Power Sources*, 2022, **538**, 231563, DOI: 10.1016/j.jpowsour.2022.231563.
15. Z. Li, X. Lin, W. Xi, M. Shen, B. Gao, Y. Chen, Y. Zheng and B. Lin, *Appl. Surf. Sci.*, 2022, **593**, 153446, DOI: 10.1016/j.apsusc.2022.153446.
16. L. Cao, Y. Wang, Q. Zhu, L. Fan, Y. Wu, Z. Li, S. Xiong and F. Gu, *ACS Applied Materials & Interfaces*, 2022, **14**, 17249-17258, DOI: 10.1021/acsami.2c00163.
17. A. Wang, C. Zhao, M. Yu and W. Wang, *Applied Catalysis B: Environmental*, 2021, **281**, 119514, DOI: 10.1016/j.apcatb.2020.119514.
18. W. Wan, X. Liu, H. Li, X. Peng, D. Xi and J. Luo, *Applied Catalysis B: Environmental*, 2019, **240**, 193-200, DOI: 10.1016/j.apcatb.2018.08.081.
19. F. Kong, Y. Qiao, C. Zhang, R. Li, T. Cheng, A. Kong and Y. Shan, *Catalysis Science & Technology*, 2019, **9**, 3469-3481, DOI: 10.1039/C9CY00746F.
20. Y. Zhang, J. Wang, M. Alfred, P. Lv, B. Liu and Q. Wei, *J. Power Sources*, 2022, **544**, 231865, DOI: 10.1016/j.jpowsour.2022.231865.
21. X. Zheng, Y. Cao, D. Liu, M. Cai, J. Ding, X. Liu, J. Wang, W. Hu and C. Zhong, *ACS Applied Materials & Interfaces*, 2019, **11**, 15662-15669, DOI: 10.1021/acsami.9b02859.

22. K. Sheng, Q. Yi, A. L. Chen, Y. Wang, Y. Yan, H. Nie and X. Zhou, *ACS Applied Materials & Interfaces*, 2021, **13**, 45394-45405, DOI: 10.1021/acsami.1c10671.
23. J. Li, Y. Wang, Z. Yin, R. He, Y. Wang and J. Qiao, *Journal of Energy Chemistry*, 2022, **66**, 348-355, DOI: 10.1016/j.jechem.2021.08.007.
24. X. Ye, Z. Han, Q. Yan, J.-J. Feng, L.-P. Mei, L. Zhang and A.-J. Wang, *J. Power Sources*, 2021, **506**, 230225, DOI: 10.1016/j.jpowsour.2021.230225.
25. Z. Zhu, Q. Xu, Z. Ni, K. Luo, Y. Liu and D. Yuan, *ACS Sustainable Chemistry & Engineering*, 2021, **9**, 13491-13500, DOI: 10.1021/acssuschemeng.1c04259.